Model-Free Sliding Mode Control of Permanent Magnet Linear Synchronous Motor Using Dynamic Gain Time Delay Estimation

Lijun Wang, Jiwen Zhao, *Senior Member, IEEE*, Juncai Song, *Member, IEEE*, Zixiang Yu, *Member, IEEE*, and Zhenbao Pan, *Member, IEEE*

***Abstract*—This article proposes a model-free sliding mode control using dynamic gain time delay estimation (DGTDE) to improve the position tracking performance of permanent magnet linear synchronous motor (PMLSM). First, an abstract order model of PMLSM is established, which eliminates the motor parameters and nonlinear terms in the conventional dynamic model. On this basis, a nonsingular fast terminal sliding mode manifold is designed to guarantee the high precision convergence of the system in finite time. Then, the lumped disturbance is simply obtained using the DGTDE method and feed-forward compensation is made to the control loop. The proposed control gain adaptive algorithm can adjust itself online based on tracking errors, thereby balancing the comprehensive control performance of the system under uncertainties. Overall, the proposed method is model free, robust, and adaptive. Finally, comparative experimental results under different operating conditions demonstrate the effectiveness and superiority of the proposed method.**

***Index Terms*—Dynamic gain time delay estimation (DGTDE), model-free, order model, permanent magnet synchronous linear motor (PMLSM), position control.**

I. Introduction

UNLIKE the conventional linear servo mode which combines a rotary motor with a roller screw or a gear rack, the permanent magnet linear synchronous motor (PMLSM)-driven servo system eliminates the intermediate mechanical drive link and achieves high efficiency and high bandwidth feed drive [1], [2]. Unsurprisingly, PMLSM-driven servo systems have been widely used in many high-precision industrial applications, such as CNC machine tools, medical equipment and industrial robots. However, in the actual application process, the positioning accuracy of the servo system is greatly reduced due to the uncertainty caused by thrust ripple, payload changes and external disturbances [3], [4]. Therefore, it is imperative to design a robust position controller for PMLSM.

To obtain satisfactory position tracking control, an accurate PMLSM dynamic model is usually required. On the basis of the original dynamics, proportional integral (PI) control [5], iterative learning control (ILC) [6], model predictive control (MPC) [7] and sliding mode control (SMC) [8] are developed and applied successfully. PI control can achieve static-errorless tracking using zero-pole cancellation, yet the zero-pole cancellation method relies on accurate motor models. Also, a single PI controller structure cannot accommodate both tracking and dynamic performance. MPC provides a high bandwidth position tracking effect by predicting control output forward with system history information. Notwithstanding, sensitivity to the motor model and control delay are two recognized limitations of MPC. For repetitive motion situations, ILC can achieve complete tracking control of the reference trajectory by generating a feedforward control action that approximates the inverse dynamics of the model. However, ideal ILC is susceptible to noise and aperiodic disturbances. Alternatively, SMC has exhibited great potential in various servo driving applications due to its low dependence on the control object model, fast dynamic response and simple implementation. Nevertheless, conventional linear SMC (LSMC) can only ensure the asymptotic convergence of tracking error, which cannot always satisfy the control requirements in some high-speed servo occasions [9]. To solve this problem, Man and Yu [10] proposed a nonlinear terminal sliding mode control (TSMC) based on terminal attraction factor to achieve a finite time convergence of system errors. However, the infinite control output at the singular point limits its further application. To overcome singular problem, Feng et al. [11] developed a nonsingular TSMC (NTSMC), which successfully avoids the negative power term by adjusting the position of the system state variable. Unfortunately, when the system state is far away the equilibrium point, the system convergence speed of NTSMC is slow, even much lower than that of LSMC. For that, a fast TSMC (FTSMC) is developed by adding a linear term to NTSMC, which realizes the optimal control in time [12], [13]. The above SMC has achieved exciting results in various motor drives. But

Received 24 November 2024; revised 12 February 2025 and 31 March 2025; accepted 7 April 2025. Date of publication 14 April 2025; date of current version 30 June 2025. This work was supported in part by the National Natural Science Foundation of China under Grant 51837001, Grant 52177038, and Grant 52207044, and in part by the Fundamental Research Funds for the Central Universities under Grant JZ2024HGTB0227. Recommended for publication by Associate Editor A. Marques Cardoso. *(Corresponding author: Lijun Wang.)*

Lijun Wang and Juncai Song are with the School of Internet, Anhui University, Hefei 230601, China (e-mail: lijunwang@ahu.edu.cn; songjuncai@ahu.edu.cn).

Jiwen Zhao, Zixiang Yu, and Zhenbao Pan are with the School of Electrical Engineering and Automation, Hefei University of Technology, Hefei 230009, China (e-mail: ustczjw@hfut.edu.cn; zixiangyu@hfut.edu.cn; pzhenbao@hfut.edu.cn).

Color versions of one or more figures in this article are available at https://doi.org/10.1109/TPEL.2025.3560556.

Digital Object Identifier 10.1109/TPEL.2025.3560556

they face the common problem that the equivalent control law depends on the exact parameters of the system. Unfortunately, during the reciprocating motion of the servo system, motor parameters may mismatch and generate additional uncertainty, thereby reducing control accuracy.

For improving the suppression capability of the SMC with respect to the disturbance and uncertainty, the methods currently used can be divided into two categories. One is to utilize the robustness of SMC itself, that is, to set a switching gain that matches the lumped disturbance. However, due to the time-varying operating conditions, the boundaries of system disturbance and uncertainty are often not available in advance. Therefore, we need to set sufficient control gains based on engineering experience, but this may lead to severe chattering. Naturally, adaptive SMC (ASMC) is an optional scheme and has achieved significant control effects. Fu and Zhao [14] and Feng et al. [15] discuss ASMC based on monotonically increasing gain. The control gain in this method can increase as the disturbance increases to maintain sliding mode. However, gain overestimation will occur when system disturbances decrease. Shao et al. [16] present an ASMC based on barrier function, which can adjust the control gain according to the magnitude of the disturbance. However, the overlarge control gain near the boundary layer can easily lead to saturation of the actuator. Another category of method is to estimate the lumped disturbance in combination with the disturbance observer (DOB) and feed it forward to the control loop. In this case, the controller only needs to set a small gain to handle observation and measurement errors, effectively weakening control chattering. In the existing literature, DOB-based SMC has been applied to motor drives, such as Luenberger observer-based SMC for sensorless control of induction motor [17], extended state observer-based SMC for ac motor speed control [18] and high order sliding mode observer for linear motor servo system [19]. However, the design of different observers undoubtedly complicates the structure of the controller. Also, some observers require precise dynamic models and system parameters. Time-delay estimation (TDE) techniques have been considered as another effective method to estimate system disturbance [20], [21]. The basic idea is to approximate the uncertainty of the system through the control inputs and state variables of the previous control cycle. Generally, the TDE does not require an explicit dynamic model or rely on precise system parameters. However, most existing TDE-based control methods are strictly limited to a constant control gain, which means that a fixed gain is used in all cases. Because the control tasks and requirements of the motor are time-varying, it is usually difficult to guarantee satisfactory comprehensive control performance with a fixed control gain. Thus, the gain selection of TDE is a problem worthy of attention.

Motived by the above analysis, this article proposes a dynamic gain time delay estimation (DGTDE) based model-free sliding mode control (MFSMC) for PMLSM position loop. The proposed method utilizes equivalent motion models and TDE technology to compensate as much as possible for complex nonlinear dynamics and disturbances. In addition, the adaptive gain and FTSMC switching gain designed for TDE can effectively suppress TDE errors and adapt to PMLSM systems under different operating conditions. Compared to existing schemes, the proposed method is model free and adaptive. The main contributions are listed as follows.

1) An equivalent order model has been established to eliminate parameters and nonlinear terms in conventional PMLSM dynamic models, providing a model-free control structure. This model-free structure undoubtedly eliminates the parameter identification process in practical engineering applications and reduces the occupation of computing resources.
2) A DGTDE-based MFSMC is designed for PMLSM position loop. The proposed controller utilizes TDE technique to estimate system disturbances online and perform real-time compensation, eliminating the need for upper bound information on disturbances. Consequently, it mitigates control chattering and enhances the overall robustness of the system.
3) A sliding mode variable-based adaptive gain tuning strategy is proposed, which can generate timely control gain based on the size of the tracking error of the tracking system. Adaptive strategies can provide appropriate control efforts for PMSLM under different operating conditions to achieve optimal tracking performance.
4) The unified uniformly bounded of tracking error under the action of DGTDE-based MFSMC is analyzed based on Lyapunov theory. The effectiveness and superiority of the proposed method were verified through comparative experiments.

The rest of this article is organized as follows. Section II introduces the mathematics model and control objective of PMLSM. Section III analyzes the limitations of existing nonsingular fast terminal sliding mode (NFTSMC) position controller. Section IV provides the design of DGTDE-based MFSMC and its stability analysis. Section V discusses the comparative experimental results. Finally, Section VI concludes this article.

II. Modeling and System Descriptions

A. Mathematics Modeling of PMLSM

The mathematics model of PMLSM under the *dq* coordinate system can be expressed as [3]

$$\begin{cases} L_q \frac{di_q}{dt} = u_q - Ri_q - \frac{\pi v}{\tau} L_d i_d - \frac{\pi v}{\tau} \varphi_f \\ L_d \frac{di_d}{dt} = u_d - Ri_d + \frac{\pi v}{\tau} L_q i_q \\ F_e = \frac{3\pi}{2\tau} \left(\varphi_f i_q + (L_d - L_q) i_d i_q \right) \end{cases} \tag{1}$$

where u_d, u_q, and i_d, i_q denote voltages and currents in *dq*-axes; R stands for coil phase resistance; L_d and L_q denote inductances in *dq*-axes; v is the linear velocity of the mover; F_e is electromagnetic thrust and τ is the pole pitch.

For the surface mounted PMLSM, the *d*- and *q*-axis inductance can be considered to be approximately equal, that is, $L_d = L_q = L$, So the electromagnetic thrust of linear motor can be simplified as

$$F_e = \frac{3\pi}{2\tau} \varphi_f i_q \equiv K_f i_q \tag{2}$$

where K_f is the electromagnetic thrust coefficient. Thus, the mechanical motion model of PMLSM can be obtained as follows:

$$F_e = M\dot{v} + G_b v + G_c \text{sign}(v) + F_{\text{ripple}} + F_{\text{ext}} \tag{3}$$

where M denotes the mass of the mover; G_b and G_c represents viscous friction coefficient and Coulomb friction coefficient; F_{ext} is the external disturbing force, including load force and cable force; F_{ripple} represent thrust ripple. Sign $(\cdot)$ denotes a sign function that is formulated as follows:

$$\text{sign}(\cdot) = \begin{cases} 1, & \text{if} \cdot > 0 \\ 0, & \text{if} \cdot = 0 \\ -1, & \text{if} \cdot < 0 \end{cases}. \tag{4}$$

Combining (2) and (3), the second-order mechanical dynamics model of PMLSM is deduced as follows:

$$\ddot{x} = \frac{1}{M}\left(K_f i_q^* - G_b v - G_c \text{sign}(v) - d\right) \tag{5}$$

where x represents the position of the mover, i_q^* indicates the q-axis control input current and $d \triangleq F_{\text{ripple}} + F_{\text{ext}}$ denotes the disturbance force that cannot be accurately modeled.

Define the position tracking error:

$$e_x \triangleq x - x^* \tag{6}$$

where x^* denotes the reference position. By substituting (5) into (6), the position error dynamics of PMLSM can be obtained as

$$\ddot{e}_x = \frac{1}{M}\left(K_f i_q^* - G_b v - G_c \text{sign}(v) - d\right) - \ddot{x}^*. \tag{7}$$

Assumption: The disturbance force d of PMLSM is assumed to be bounded, that is, $|d| \le \bar{d}$ with a positive constant $\bar{d}$. This assumption holds practical relevance in the application of PMLSMs. Specifically, the disturbances experienced by PMLSMs in practical applications are typically bounded signals. For instance, in laser cutting machines or CNC tools, the thrust ripple resulting from the side-end effect of PMLSMs may vary with mover position, yet the amplitude of this ripple remains constrained. Similarly, when a CNC machine tool's end mill cuts through material, the load thrust may fluctuate with cutting depth, but the amplitude of these fluctuations is always limited [22], [23].

B. Control Objective and Description of PMLSM Servo System

Based on the error dynamic model, the control objective of this article is to drive the position tracking error to converge in a finite time under various disturbances and uncertainties. To achieve this goal, the PMLSM drive system shown in Fig. 1 is established. The whole system is composed of rectifier, inverter, control unit, encoder and PMLSM. The control unit adopts a dual-loop structure in which the position loop and the current loop are cascaded. Specifically, the proposed MFSMC is applied to position loop and outputs the reference input of the current loop. Two PI controllers are used in the current loop to generate the control voltage required to drive PMLSM. The position and velocity information are fed back through the encoder.

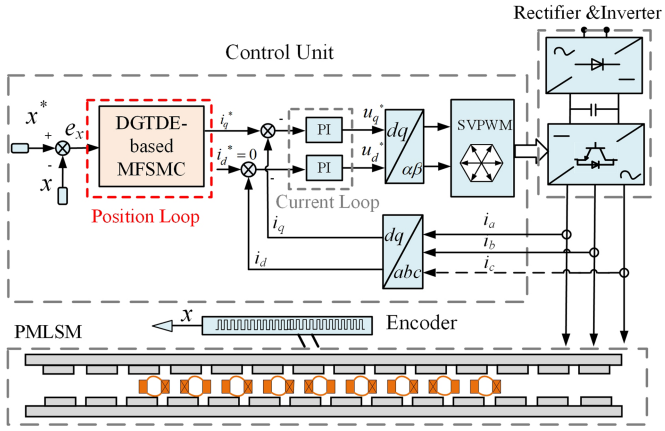

Fig. 1. Block diagram of the PMLSM-driven servo system.

III. Existing NFTSMC for PMLSM Position Loop

Generally, the design of SMC includes two steps: the selection of sliding mode manifold and the design of control law. In a recent study of SMC position controller, the following NFTSM manifold is usually selected for the second-order system in (7) [4], [12], [24]

$$s_x = \dot{e}_x + \alpha e_x + \beta \text{sig}(e_x)^{\lambda} \tag{8}$$

where $\text{sig}(\cdot)^{\lambda} = |\cdot|^{\lambda}\,\text{sign}(\cdot)$ is used to simplify expression; α, β, and λ are sliding mode parameters to be designed and meet α, $\beta > 0$ and $\lambda > 1$. Then, the design of control law includes two parts: equivalent control law $i_{q(eq)}^*$ and sliding mode switching control law $i_{q(sw)}^*$.

First, assuming that there is no disturbance force in the PMLSM-driven servo system, that is, $d = 0$, the equivalent control law can be obtained by making $s_x = 0$. Accordingly, it obtains

$$i_{q(\text{eq})}^* = \frac{M}{K_f}\left(\ddot{x}^* - \alpha\dot{e}_x - \beta\lambda|e_x|^{\lambda-1}\dot{e}_x\right) + \frac{G_b v + G_c \text{sign}(v)}{K_f}. \tag{9}$$

Second, select the well-known exponential reaching law [25] to achieve the fast convergence of the system. Combining (8), the switching control law can be obtained as

$$i_{q(\text{sw})}^* = -\frac{M}{K_f}\left(k_1 s_x + k_2 \text{sign}(s_x)\right) \tag{10}$$

where $k_1 > 0$ and $k_2 > 0$ are control gains to be designed.

Finally, the whole control law is deduced as

$$\begin{aligned} i_q^* &= i_{q(\text{eq})}^* + i_{q(\text{sw})}^* \\ &= \frac{M}{K_f}\left(\ddot{x}^* - \alpha\dot{e}_x - \beta\lambda|e_x|^{\lambda-1}\dot{e}_x + \frac{G_b v + G_c \text{sign}(v)}{M}\right. \\ &\quad \left. - k_1 s_x - k_2 \text{sign}(s_x)\right). \end{aligned} \tag{11}$$

To guarantee the system stability conditions: $s_x \dot{s}_x < 0$, the selection of control gain must satisfy $k_2 > M^{-1}\bar{d}$. Under this condition, the conventional NFTSMC can improve the robust performance and tracking performance of PMLSM to certain extent. However, this method faces two problems.

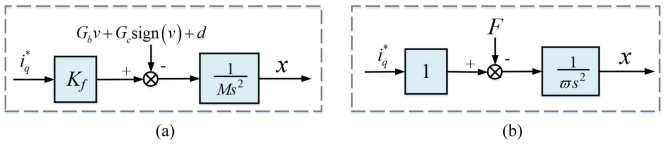

Fig. 2. Frequency domain block diagram of PMLSM model. (a) Original model. (b) Order model.

1) In practice, the boundary $\bar{d}$ of disturbance force is difficult to obtain in advance. Thus, we can only select a sufficiently large gain k_2 based on engineering experience to achieve the sliding mode. Once the disturbance is reduced, the constant k_2 will lead to the overestimation problem. And the term k_2 sign(s) in (11) will cause severe chattering.
2) From (9), the equivalent control law $i_{q(eq)}^*$ involves motor parameters M, K_f, G_c, and G_b. This means that the effect of desired dynamics depends on the accuracy of the system parameters. System parameters mismatch will introduce additional uncertainty and further reduce tracking accuracy of PMLSM drive.

IV. Proposed Position Controller Design

To overcome the above problems, this section proposes a new PMLSM position controller. The controller mainly includes the design of MFSMC and DGTDE.

A. Proposed DGTDE-Based MFSMC Design

1) Design of MFSMC: From (5), we can observe that the original PMLSM position dynamics incorporated motor parameters M, K_f, G_c, and G_b. The SMC law (11) developed using this model also incorporated these parameters. To mitigate the impact of variations in these parameters, we have reconstructed the dynamic model by considering solely the system's order. Substituting (2) into (3) yields

$$i_q^* = \frac{M}{K_f}\ddot{x} + \frac{1}{K_f}\left(G_b v + G_c \text{sign}\left(v\right) + d\right). \tag{12}$$

Further introducing non-physical parameter ϖ, (12) can be rewritten as the following order model:

$$i_q^* = \varpi\ddot{x} + F \tag{13}$$

where $F = \frac{M}{K_f}\ddot{x} - \varpi\ddot{x} + \frac{1}{K_f}(G_b v + G_c \text{sign}(v) + d)$.

It is worth noting that the term F encompasses all uncertain and unknown dynamic factors, including friction, thrust ripple, and other external disturbance forces. There is no need to make any distinction between them. In contrast to the original dynamic model, the order model presented in (13) relies solely on the fundamental order characteristics of the system, achieving parameter independence. As depicted in Fig. 2, we observe that the transfer function forms of both the original model and the order model are consistent, thereby demonstrating the feasibility of the equivalent order model in accurately describing the positional dynamics of the PMLSM.

To facilitate the analysis below, the proposed order model can be rewritten as

$$\ddot{x} = \frac{1}{\varpi}\left(i_q^* - F\right). \tag{14}$$

Accordingly, the position error dynamics can be rewritten as

$$\ddot{e}_x = \varpi^{-1}\left(i_q^* - F\right) - \ddot{x}^*. \tag{15}$$

For the sake of generality, this article adopts the same sliding mode manifold as (8). Then, the design of MFSMC control law is divided into three steps.

First, to achieve the desired error dynamics in NFTSM manifold, that is

$$\ddot{e}_x + \alpha\dot{e}_x + \beta\lambda|(\dot{e}_x)|^{\lambda-1}\dot{e}_x = 0. \tag{16}$$

We design the following equivalent control law $i_{q(eq)}^*$ by substituting (15) into (16) and letting $F = 0$

$$i_{qeq}^* = \varpi\left(\ddot{x}^* - \alpha\dot{e}_x - \beta\lambda|(\dot{e}_x)|^{\lambda-1}\dot{e}_x\right). \tag{17}$$

Next, the compensation of lumped disturbance F is further considered. Instead of directly using the switching control in the conventional SMC, the TDE method is used to estimate F in this article. More specifically, we have

$$\hat{F} = F_{(t-T_s)} = i_{q(t-T_s)}^* - \varpi\ddot{x}_{(t-T_s)} \tag{18}$$

where $\hat{F}$ is the estimated value of F; $F_{(t\text{-}Ts)}$, $i_{q(t\text{-}Ts),}^*$ and $\ddot{x}_{(t\text{-}Ts)}$ indicate the value in previous sampling period; T_s is the sampling period and the smaller the value, the more accurate the estimation result of (18) [21], [26]. Note that the delay involved in (18) is intentionally designed to estimate the lumped disturbance of PMLSM, rather than the conventional physical delay of the controlled plant [27].

By substituting (17) and (18) into (16), the actual close-loop error dynamics can be derived as follows:

$$\varpi\left(\ddot{e}_x + \alpha\dot{e}_x + \beta\lambda|\dot{e}_x|^{\lambda-1}\dot{e}_x\right) = \hat{F} - F. \tag{19}$$

Obviously, if $\hat{F} = F$, (19) is equivalent to (16), which means that the system can achieve the desired dynamics under the action of (17) and (18). Unfortunately, in the actual PMLSM drive, measurement noise and limited sampling time can result in $\hat{F} \neq F$. Define the TDE estimation error: $\varepsilon \triangleq \hat{F} - F$. Then the actual close-loop error dynamics in (19) can be rewritten as

$$\left(\ddot{e}_x + \alpha\dot{e}_x + \beta\lambda|\dot{e}_x|^{\lambda-1}\dot{e}_x\right) = \frac{\varepsilon}{\varpi}. \tag{20}$$

Aiming to reduce the impact of TDE errors, we introduce the following error suppression terms:

$$i_{q(\text{sw})}^* = -\varpi\left(k'_1 s_x + k'_2 \text{sign}\left(s_x\right)\right) \tag{21}$$

where $k'_1 > 0$ and $k'_2 > 0$ are control gains. It can be seen that the form of the TDE error suppression term is similar to the conventional sliding mode switching control law. The difference is that the gain k'_1 and k'_2 in (21) only needs to handle the estimation error ε. Therefore, k'_1 and k'_2 are much smaller than the gain k_1, k_2 of directly processing lumped disturbances in (10).

Combining (17), (18), and (21), the entire control law of MFSMC is derived as

$$\begin{aligned} i_q^* &= i_{q(\text{eq})}^* + \hat{F} + i_{q(\text{sw})}^* \\ &= \varpi\left(\ddot{x}^* - \alpha\dot{e}_x - \beta\lambda|(e_x)|^{\lambda-1}\dot{e}_x - k'_1 s_x - k'_2 \text{sign}\,(s_x)\right) \\ &\quad + i_{q(t-T_s)}^* - \varpi\ddot{x}_{(t-T_s)}. \end{aligned} \tag{22}$$

From (22), control law of MFSMC does not contain any motor system parameters and provides a model-free control effort. Also, the control gain only needs a small value to handle the TDE error, which reduces the inherent chattering. Overall, the proposed MFSMC overcomes the shortcomings of conventional SMC mentioned earlier to certain extent.

2) Effect of Gain ϖ: As the TDE is an estimation technique, the limited sampling time and discontinuous friction in practical applications can inherently lead to estimation errors [28], which significantly affect the stability and performance of closed-loop systems. To ensure the boundedness of TDE errors, the parameter ϖ needs to satisfy the following condition:

$$|1 - \varpi K_f/M| < 1. \tag{23}$$

The detailed proof is given in Appendix A. The boundedness of ε is also an important prerequisite for the subsequent stability analysis of Section III-C.

In addition, the acceleration term $\ddot{x}_{(t\text{-}T)}$ in (22) will cause serious control noise. Fortunately, adjusting the gain ϖ can effectively reduce this phenomenon. More specifically, (22) can be rewritten as

$$i_q^* = \varpi\left(\Gamma - \ddot{x}_{(t-T_s)}\right) + i_{q(t-T_s)}^* \tag{24}$$

$$\text{with}\,\Gamma = \ddot{x}^* - \alpha\dot{e}_x - \beta\lambda|(\dot{e}_x)|^{\lambda-1}\dot{e}_x - k'_1 s_x - k'_2 \text{sign}\,(s_x)\,. \tag{25}$$

If an additional digital low-pass filter is introduced, the control law can be rederived as

$$i_{qf}^* = \frac{\omega'}{1+\omega'} i_q^* + \frac{1}{1+\omega'} i_{qf(t-T_s)}^* \tag{26}$$

where $\omega' = \omega T_s$, ω is the cutoff frequency of low-pass filter and i_{qf}^* is the output of filter. Substituting (24) into (26), it obtains

$$i_{qf}^* = \frac{\omega'}{1+\omega'}\varpi\left(\Gamma - \ddot{x}_{(t-T_s)}\right) + i_{qf\,(t-T_s)}^*. \tag{27}$$

Obviously, a small ϖ can be equivalent to the effect of a low-pass filter. Therefore, the control system does not need to configure additional low-pass filters.

Combining (20) and (27), it is not difficult to find that the selection of ϖ is a tradeoff between suppressing signal noise and reducing TDE error. Specifically, if a large control gain ϖ is improperly used, serious noise effects can occur, even fail to meet the stability condition in (23) and cause the control system to be unstable. Conversely, if the control gain ϖ is chosen too small, the control accuracy may deteriorate, even failing to track the desired trajectory. Due to the time-varying control tasks and requirements of motors, it is often difficult to ensure good comprehensive control performance using a fixed control gain ϖ in MFSMC. A dynamic gain configuration to the MFSMC is required to adapt to various operating conditions of the PMLSM and achieve strong anti-interference capabilities.

3) Design of DGTDE: To improve the adaptability and guarantee excellent tracking performance of MFSMC, we propose the following dynamic gain for ϖ

$$\begin{cases} \dot{\hat{\varpi}} = c\,|s_x|\,e^{|s_x|}\text{sign}\,(|s_x| - \sigma)\,, \hat{\varpi} \geq \varpi_0 \\ \hat{\varpi} = \varpi_0, \hat{\varpi} < \varpi_0 \end{cases} \tag{28}$$

where c and σ are positive parameters to be designed. ϖ_0 is a small value to avoid negative $\hat{\varpi}$.

Next, let's describe the mechanism of adaptive dynamic gain: when the system is subject to disturbance changes, the estimation error ε increases. According to (8) and (20), the position tracking error e_x and sliding mode variable s_x increase accordingly. Once $s_x > \sigma$, $\hat{\varpi}$ continues to increase and drive e_x to gradually decrease. When e_x is small enough, s_x is also smaller, resulting in $s_x < \sigma$. In this case, sign(|s_x|-σ) $= -1$, $\hat{\varpi}$ begins to decrease continuously. Once $\hat{\varpi} < \varpi_0$, $\hat{\varpi}$ starts adjusting again based on the first term of (28). It is visible that $\hat{\varpi}$ can be adaptively adjusted according to the change of s_x (equivalent to the change of e_x) to obtain excellent comprehensive tracking performance under different working conditions.

By configuring the designed dynamic gain $\hat{\varpi}$ in the original TDE and MFSMC, the control law of DGTDE-based MFSMC can be obtained as follows:

$$\begin{aligned} i_q^* &= \hat{\varpi}\left(\ddot{x}^* - \alpha\dot{e}_x - \beta\lambda|(e_x)|^{\lambda-1}\dot{e}_x - k'_1 s_x - k'_2 \text{sign}\,(s_x)\right) \\ &\quad + i_{q(t-T_s)}^* - \hat{\varpi}\ddot{x}_{(t-T_s)}. \end{aligned} \tag{29}$$

To gain further insight into the proposed method, we have presented the structure block diagrams of NFTSMC, original TDE-based MFSMC and DGTDE-based MFSMC, respectively, as shown in Fig. 3. Obviously, compared to existing NFTSMC, the control loops of TDE-based MFSMC and DGTDE-based MFSMC no longer contain any motor parameters (M, K_f, G_c, and G_b) and are model-free structures. For TDE-based MFSMC and DGTDE-based MFSMC, it can be seen that if the dynamic gain tuning loop in Fig. 3(c) is removed, the two diagrams will be identical. The purpose of equivalent control law is to inject the desired error dynamics into the PMLSM dynamics. Switching control law is intended to initially suppress TDE estimation error ε. Both TDE and DGTDE can eliminate the influence of lumped disturbance. The difference is that the additional adaptive $\hat{\varpi}$ dynamics can use sliding variables s_x to monitor tracking errors and automatically adjust the gain $\hat{\varpi}$, which possess a stronger ability to resist disturbances.

Remark 1: Compared to state-of-the-art SMC [29], [30], [31], the improvement of the proposed method lies in the fact that the equivalent control law no longer relies on any motor parameters and provides model-free control. This substantial enhancement is primarily attributed to the design of the novel dynamic order model detailed in (14). On the other hand, compared to the commonly used observer method for suppressing system uncertainty [32], [33], the DGTDE designed in this article does not require disturbance to be continuously differentiable, but only requires the input and output of the system at the previous moment. Moreover, the design of dynamic gain $\hat{\varpi}$ in (28) also overcomes the

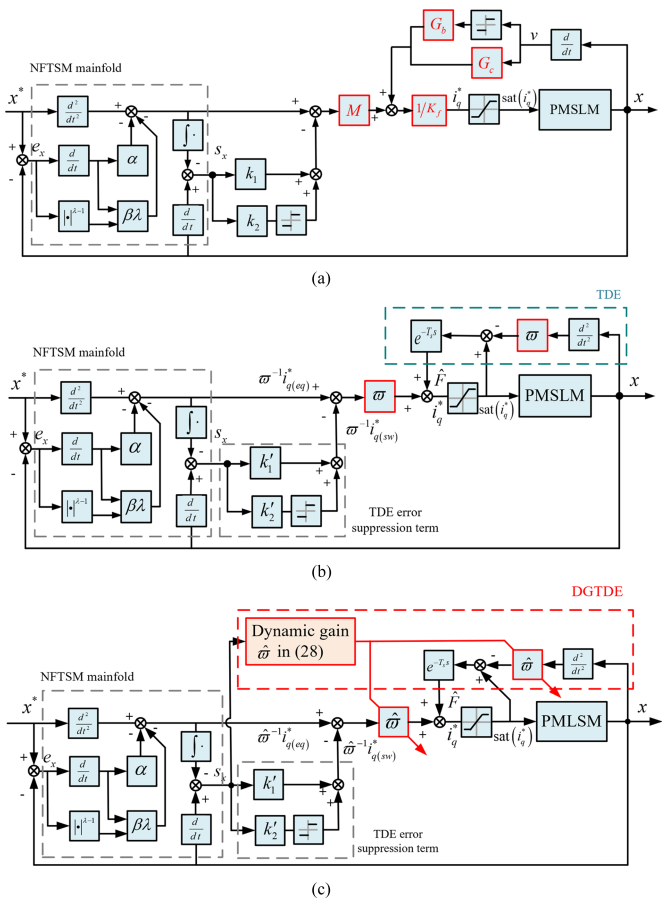

Fig. 3. Block diagram of three methods. (a) Existing NFTSMC. (b) Original TDE-based MFSMC. (c) DGTDE-based MFSMC.

limitations of fixed gain in existing TDE-based SMC [21]. This design improvement augments the comprehensive performance of the controller under varying operating conditions.

Remark 2: It is worth noting that the model-free SMC proposed in this article primarily addresses the position loop control of PMLSM, whereas the research in [34] focuses on speed loop control. The model discussed herein possesses a higher order and necessitates further consideration of noise issues arising from the quadratic differentiation of state variables. This article tackles this problem through the equivalent filtering effect of DGTDE. Additionally, a variable-gain model-assisted linear expansion observer (TMLESO) presented in [34] is used to estimation disturbance, which relies on the assumption of continuous differentiability of disturbances. In contrast, the DGTDE utilized in this article removes this constraint and offers a relatively broader range of applicability. In terms of chattering suppression, the adaptive boundary layer method introduced in [34] effectively mitigates chattering associated with SMC, providing valuable insights for subsequent research of this article.

B. Stability Proof

Lemma 1: For the PMLSM system (15) and control law (29), the adaptive gain $\hat{\varpi}$ has an upper bound $\bar{\varpi}$, that is $\hat{\varpi} < \bar{\varpi}$, for $t \geq 0$. The proof is given in Appendix B.

To prove the stability of the closed-loop system under the control law of (29), we define the following Lyapunov function:

$$V = \frac{1}{2}{s_x}^2 + \frac{1}{2}\mu(\hat{\varpi} - \bar{\varpi})^2 \tag{30}$$

where μ is positive constant. Tacking the derivative of V with respect to time, it can obtain

$$\begin{aligned}\dot{V} &= s_x\dot{s}_x +]!\mu\left(\hat{\varpi} - \bar{\varpi}\right)\dot{\hat{\varpi}} \\ &= s_x\left(\varpi^{-1}\left(i_q^* - F\right) - \ddot{x}^* + \alpha\dot{e}_x + \beta\lambda|e_x|^{\lambda-1}\dot{e}_x\right) + \mu\left(\hat{\varpi} - \bar{\varpi}\right)\dot{\hat{\varpi}} \\ &= \frac{\varepsilon}{\hat{\varpi}}s_x - k'_1 s_x^2 - k'_2\left|s_x\right| + \mu\left(\hat{\varpi} - \bar{\varpi}\right)c\left|s_x\right|e^{|s_x|}\mathrm{sign}\left(|s_x| - \sigma\right) \\ &\leq \left(\frac{\varepsilon}{\hat{\varpi}} - k'_2\right)\left|s_x\right| - k'_1 s_x^2 + \mu\left(\hat{\varpi} - \bar{\varpi}\right)c\left|s_x\right|e^{|s_x|}\mathrm{sign}\left(|s_x| - \sigma\right).\end{aligned} \tag{31}$$

Since ε and $\hat{\varpi}$ are bounded, we can choose the control gain k'_2 to satisfy $k'_2 > \max\{\varepsilon/\hat{\varpi}\}$. In this case, we have

$$\dot{V} \leq -k'_1 s_x^2 + \mu\left(\hat{\varpi} - \bar{\varpi}\right)c\left|s_x\right|e^{|s_x|}\mathrm{sign}\left(|s_x| - \sigma\right). \tag{32}$$

Due to the existence of symbolic function sign $(\cdot)$, we consider two cases: $s_x > \sigma$ and $s_x < \sigma$. For the case of $s_x > \sigma$: According to *Lemma 1*, it can obtain $\hat{\varpi} < \bar{\varpi}$. Thus, we have $\mu(\hat{\varpi} - \bar{\varpi})c|s_x|e^{|s_x|}\mathrm{sign}(|s_x| - \sigma) < 0$ that yields

$$\dot{V} \leq -k'_1 s_x^2. \tag{33}$$

Clearly, V will continue to decrease, causing sliding mode variables to enter the set: $\{s_x | s_x < \sigma\}$. For the case of $s_x < \sigma$: we have

$$\dot{V} \leq -k'_1 s_x^2 + \mu\left(\bar{\varpi} - \hat{\varpi}\right)c\left|s_x\right|e^{|s_x|}. \tag{34}$$

Since $\mu(\bar{\varpi} - \hat{\varpi})c|s_x|e^{|s_x|} > 0$, $\dot{V}$ is indefinite. This means that s_x will escape from the set: $\{s_x | s_x < \sigma\}$ and return to the case of $s_x > \sigma$. Therefore, we can obtain the upper bound of V as follows:

$$\frac{1}{2}s_x^2 \leq V \leq \frac{1}{2}\sigma^2 + \frac{1}{2}\max\left\{\mu\left(\bar{\varpi} - \hat{\varpi}\right)c\left|s_x\right|e^{|s_x|}\right\}. \tag{35}$$

Furthermore, we can conclude that s_x is bounded by

$$|s_x| \leq \sqrt{\sigma^2 + \max\left\{\mu\left(\bar{\varpi} - \hat{\varpi}\right)c\left|s_x\right|e^{|s_x|}\right\}} \triangleq \Omega. \tag{36}$$

To this end, the bounded proof of the sliding mode variable s_x is completed. For further analyze the convergence of system tracking error e_x, we also consider the following two different cases.

Case 1: Rewrite (8) as the following form:

$$\dot{e}_x + \alpha e_x + \left[\beta - \frac{s_x}{\mathrm{sig}(e_x)^\lambda}\right]\mathrm{sig}(e_x)^\lambda = 0. \tag{37}$$

It can be seen that (37) still holds the form of (8) and shares the same convergence characteristic as long as $\beta - s_x/\mathrm{sig}(e_x)^\lambda > 0$ is satisfied [35]. This means that the tracking error will converge to the region with $|e_x| \leq (\Omega/\beta)^{1/\lambda}$. Then, for the system

$$\dot{e}_x = -\alpha e_x - \beta'\mathrm{sig}(e_x)^\lambda \tag{38}$$

where $\beta' = \beta - s_x/\text{sig}(e_x)^\lambda$. Define the Lyapunov function $V = \frac{1}{2}e_x^2$ and the derivative of V to time can be obtained as

$$\dot{V} = e_x\dot{e}_x = -\alpha e_x^2 - \beta'|e_x|^{\lambda+1}$$
$$\leq -\left(\alpha|e_x| + \beta'|e_1|^\lambda\right)\sqrt{2}\frac{|e_x|}{\sqrt{2}} = -\sqrt{2}\Gamma_1 V^{\frac{1}{2}} \quad (39)$$

where $\Gamma_1 = \alpha|e_x| + \beta'|e_x|^\lambda$. According to the finite time stability theory given in Appendix C, the time for the tracking error e_x to converge to $|e_x| \leq (\Omega/\beta)^{1/\lambda}$ satisfies

$$t_e \leq \frac{\sqrt{2}V^{\frac{1}{2}}(0)}{\Gamma_1}. \quad (40)$$

Case 2: Alternatively, rewrite (8) as the following form:

$$\dot{e}_x + \left(\alpha - \frac{s_x}{e_x}\right)e_x + \beta\text{sig}(e_x)^\lambda = 0. \quad (41)$$

Similar to the derivation method in case 1, we can easily obtain that the error will converge to the region $|e_x| \leq \Omega/\alpha$, and the convergence time satisfies

$$t_e \leq \frac{\sqrt{2}V^{\frac{1}{2}}(0)}{\Gamma_2} \quad (42)$$

where $\Gamma_2 = (\alpha - s_x/e_x)|e_x| + \beta|e_x|^\lambda$.

Finally, it can be concluded that the tracking error under the proposed control law (29) will converge to the bounded region given by

$$|e_x| \leq \max\left\{\left(\frac{\Omega}{\beta}\right)^{\frac{1}{\lambda}}, \frac{\Omega}{\varepsilon}\right\} \quad (43)$$

in the finite time

$$t_e \leq \sqrt{2}V^{\frac{1}{2}}(0)\max\left\{\frac{1}{\Gamma_1}, \frac{1}{\Gamma_2}\right\}. \quad (44)$$

This completes the proof of finite time convergence of the position tracking error.

C. Parameters Tuning of Controller

It is essential to highlight that the selection of controller parameters plays a critical role in achieving satisfactory servo performance for the PMLSM system. During implementation, practitioners must strike a balance between desired tracking performance and various factors such as control input saturation, control signal chattering, and measurement noise. In this section, we discuss the parameter selection criteria for the proposed DGTDE-based MFSMC.

1) *Tuning Criteria of* α, β, *and* λ: The selection of α, β, and λ should adhere to the defined range ($\alpha > 0, \beta > 0, \lambda > 1$) to avoid control input singularity. These parameters also determine the dynamic performance of the sliding mode function S_x. Larger values accelerate the convergence of the tracking error to zero. However, caution must be exercised to prevent excessively high values that may lead to control input saturation.
2) *Tuning Criteria of* c, σ, and ϖ_0: The parameters c in (28) influence the adaptive rate of the dynamic gain. Higher values facilitate a more effective adaptive rate, but excessively large values can cause the gain to overshoot the stable region, potentially leading to system divergence. It is advisable to gradually increase these parameters from smaller values during the actual tuning process. Meanwhile, the parameter σ plays a crucial role in balancing tracking performance and chattering suppression. If σ is too small, the system may exhibit significant chattering due to slow adaptation speed. Conversely, if σ is too large, tracking performance may be compromised. Fortunately, the presence of the acceleration term $c|s_x|e^{|s_x|}$ in the proposed adaptive law offers flexibility in selecting σ. As for the lower bound of $\hat{\varpi}$, the parameter ϖ_0 can be arbitrarily set as a small normal number without requiring manual adjustment through trial and error.
3) *Tuning Criteria of* k'_1 and k'_2: The parameters k'_1 and k'_2 in the TDE error suppression terms can be set to smaller values since they are primarily responsible for handling the estimation error of TDE. It is recommended to gradually decrease these parameters from larger values during the tuning process until the tracking error begins to significantly increase.

Remark 3: It is worth noting that although the parameter tuning criterion cannot directly determine the optimal combination of control parameters, it can enhance the overall tuning efficiency. The determination of the final parameter set depends on the actual control performance. When further parameter adjustments no longer result in significant improvement in position tracking accuracy, debugging may be concluded. In practical engineering applications, specific position tracking accuracy indicators can serve as termination criteria for debugging. In addition, optimization algorithms such as neural networks, genetic algorithms, and differential evolution algorithms can directly obtain the optimal combination of control parameters; however, their implementation may increase the computational burden on the control system and diminish its dynamic response capabilities.

TABLE I
PARAMETERS OF PMLSM

Parameters	Symbol	Values
d-frame inductance	L_d (H)	0.004
q-frame inductance	L_q (H)	0.004
Mover mass	M (kg)	1.88
PM flux	φ_f(Wb)	0.0924
Mover winding resistance	R (Ω)	3.62
Pole pitch	τ (m)	0.0237
Viscous friction	G_b (N.s/m)	9.36
Coulomb friction	G_c (N)	12.5

V. EXPERIMENTAL RESULTS

The proposed method is validated by the PMLSM experimental platform shown in Fig. 4. The main parameters of the tested PMLSM are listed in Table I. The PMLSM is driven through a driver board, which mainly includes an intelligent power module module, two Hall sensors, six optocoupler isolation circuits,

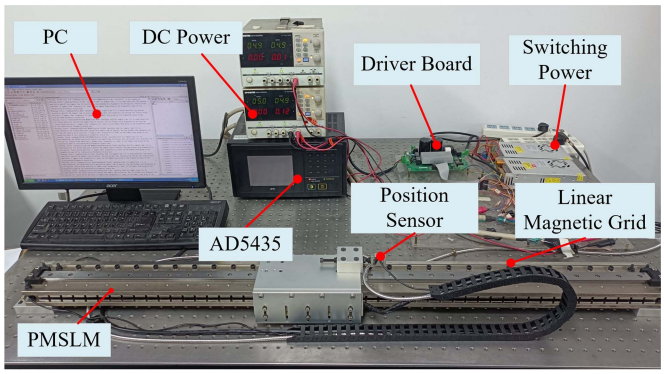

Fig. 4. Experimental setup of PMLSM servo control system.

TABLE II
PARAMETERS OF THREE CONTROLLERS

Control Methods	Parameters Values
NFTSMC (M1)	α=100, β=2, λ=2.5, k_1= k_2 =25
TDE-based MFSMC (M2)	α=100, β=2, λ=2.5, $k_1' = k_2'$ =5, ϖ =0.1
DGTDE-based MFSMC (M3)	α=100, β=2, λ=2.5, $k_1' = k_2'$ =5, c=4, σ=0.05, ϖ_0=0.05

overcurrent protection circuits, and rectification modules. Direct current power supply and switching power supply are used for power supply of the drive circuit. The magnetic grating encoder with accuracy of 5 μm is installed in parallel with the motor guide rail to realize the feedback of position information. Ad5435 hardware in the loop system is used to execute control algorithm, enhanced quadrature encoder pulse decoding, analog-to-digital converter, digital-to-analog converter (DAC) and Space Vector Pulse Width Modulation (SVPWM). The experimental results are transmitted to the upper computer interface for real-time display after DAC.

For comparison, a series of experiments were carried out in three methods shown in Fig. 3, namely existing NFTSMC method (denoted as M1), TDE-based MFSMC method (denoted as M2) and DGTDE-based MFSMC method (denoted as M3). For fair comparison, all the control parameters are first obtained from preliminary simulation and ultimately determined when satisfactory transient and steady-state performance is achieved under similar maximum control input amplitudes in the experiment. Specifically, for the parameters k_1 and k_2 in NFTSMC, they are gradually increased from zero until the control chattering reaches a significant increase and then stabilizes. This approach minimizes tracking error without overestimating disturbance. Regarding the parameter ϖ in TDE-based MFSMC, it serves as a weight factor to reduce both tracking error and inhibitory control noise. Its value is constrained by (23). It is recommended to start with a smaller value and gradually increase it until the amplitude of the control input exceeds that of NFTSMC. Through this iterative process of trial and error, a relatively optimal value of the control gain ϖ can be determined. The detailed parameter selection is given in Table II.

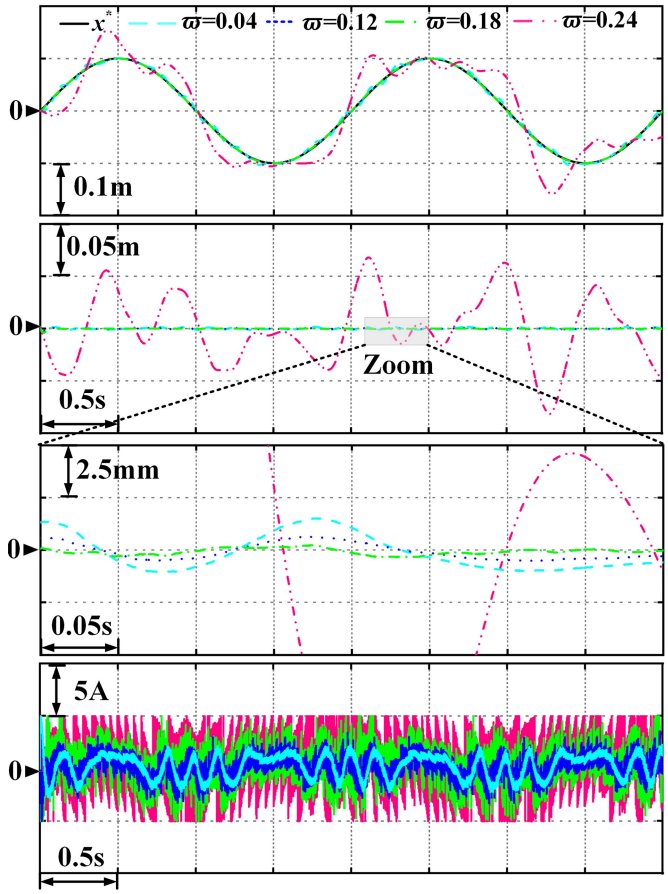

Fig. 5. Experimental results under various constant gains. From top to bottom: position trajectory $x^*$and x, position tracking error e_x, local amplification of positional errors and control input current i_q^*.

A. TDE-Based MFSMC With Various Constant Gains

To evaluate the impact of TDE convergence on PMSLM systems and the limitations of constant gain on TDE-based MFSMC, we systematically varied the parameter ϖ as 0.04, 0.12, 0.18, and 0.24. The experimental results for these different gains are visually presented in Fig. 5. It is evident that an appropriate increase in ϖ can effectively reduce tracking error, but it also introduces amplified control noise. Nonetheless, when ϖ reaches 0.24, the constraint specified in (23) is violated, resulting in severe control chattering and gradual divergence of the TDE error, ultimately leading to system instability. Encouragingly, these empirical findings substantiate the theoretical analysis outlined in the "*Tuning of Gain* ϖ" section. In light of these results, it is evident that relying solely on a constant gain may not suffice to accommodate the diverse demands imposed by various operating conditions in practical applications.

B. Steady-State Performance Verification

Figs. 6 and 7 show the experimental results of three comparison methods under sinusoidal position reference trajectories with frequencies 6.28 and 3.14 rad/s. It should be noted that

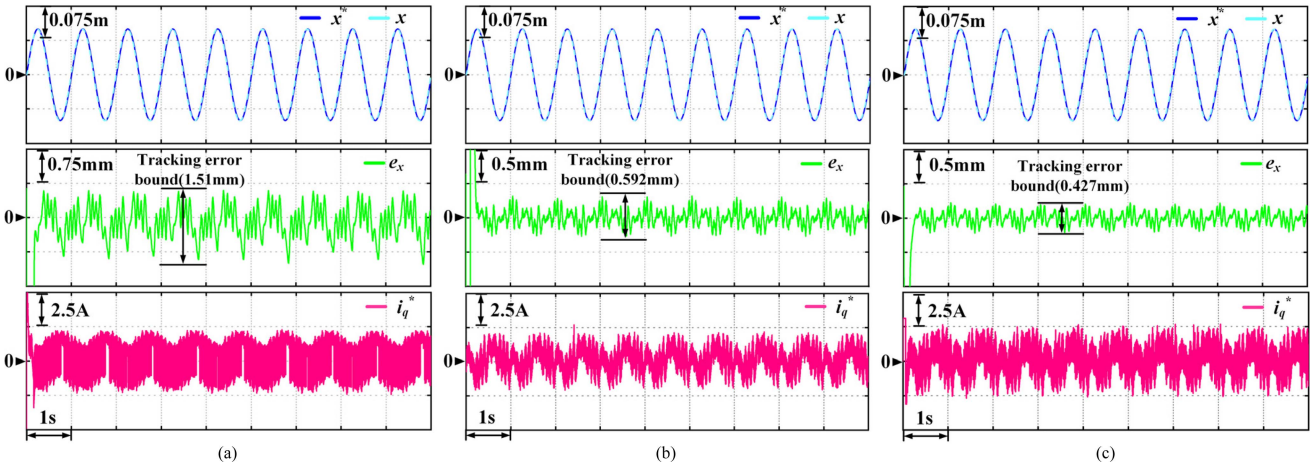

Fig. 6. Experimental results of three methods under sinusoidal position command with a frequency of 6.28 rad/s. From top to bottom: position trajectory $x^*$and x, position tracking error e_x and control input current i_q^*. (a) Existing NFTSMC: (M1). (b) TDE-based MFSMC: (M2). (c) DGTDE- based MFSMC: (M3).

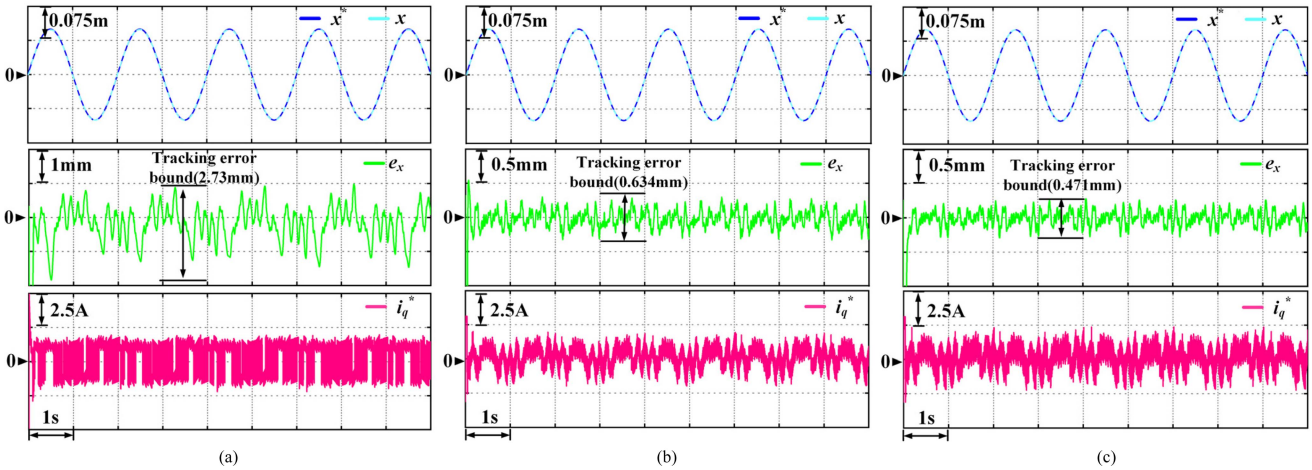

Fig. 7. Experimental results of three methods under sinusoidal position command with a frequency of 3.14 rad/s. From top to bottom: position trajectory $x^*$and x, position tracking error e_x and control input current i_q^*. (a) Existing NFTSMC: (M1). (b) TDE-based MFSMC: (M2). (c) DGTDE-based MFSMC: (M3).

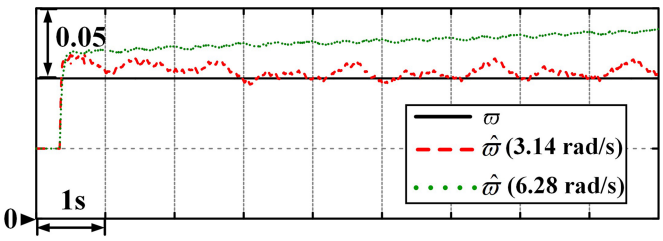

Fig. 8. Gains of TDE-based MFSMC and DGTDE- MFSMC.

in this case, the PMLSM servo system is primarily affected by disturbances such as thrust ripple and friction force.

For the existing NFTSMC method, the position response curves can basically track the desired command from Figs. 6(a) and 7(a). However, due to uncertainties such as thrust ripple and friction, NFTSMC generates significant tracking errors shown in Figs. 6(b) and 7(b). Specifically, the tracking error bound (TEB) of NFTSMC are 1.51 and 2.73 mm at 6.28 and 3.14 rad/s, respectively. In addition, the chattering of the control input current of NFTSMC is very obvious from Figs. 6(c) and 7(c). This is because larger control gain k_1 and k_2 are needed to ensure the tracking accuracy and robustness of the system. Unsurprisingly, this result is also consistent with the previous limitation analysis of NFTSMC.

For the TDE-based MFSMC method, its TEB decreased to 0.592 and 0.634 mm at 6.28 and 3.14 rad/s, respectively. Compared with NFTSMC, the TEB of TDE-based MFSMC decreased by 60.79% and 76.78%. Obviously, TDE-based MFSMC has better steady-state tracking performance. On the other hand, the chattering of the control input current of TDE-based MFSMC has been weakened shown in Figs. 6(b) and 7(b). This is because the switching gain k'_1 and k'_2 in TDE-based MFSMC only needs to be set to a smaller value to handle the estimation error of TDE. However, since the gain ϖ in MFSMC is

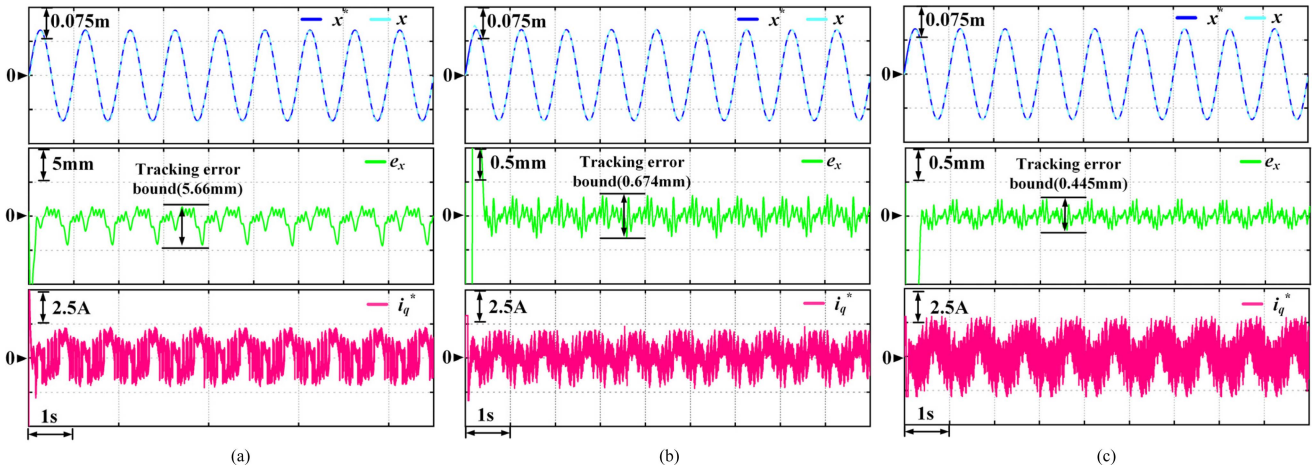

Fig. 9. Experimental results of three methods under parameter mismatch: $\Delta M = M$, $\Delta K_f = 0.2K_f$, $\Delta G_c = G_c$, and $\Delta G_b = G_b$ (sinusoidal position command with a frequency of 6.28 rad/s). From top to bottom: position trajectory $x^*$and x, position tracking error e_x and control input current i_q^*. (a) Existing NFTSMC: (M1). (b) TDE-based MFSMC: (M2). (c) DGTDE- MFSMC: (M3).

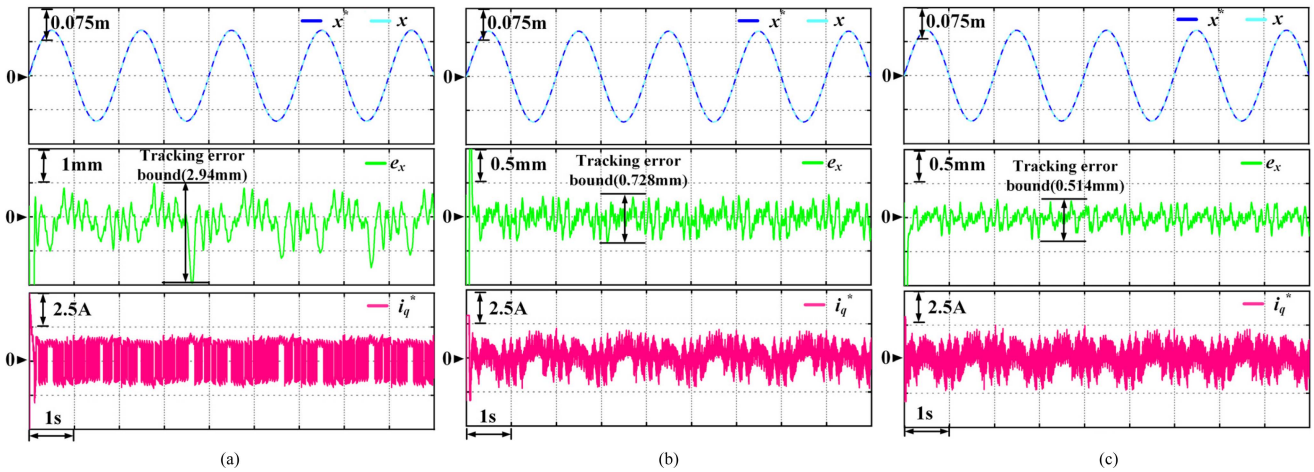

Fig. 10. Experimental results of three methods under parameter mismatch: $\Delta M = M$, $\Delta K_f = 0.2K_f$, $\Delta G_c = G_c$, and $\Delta G_b = G_b$ (sinusoidal position command with a frequency of 3.14 rad/s). From top to bottom: position trajectory $x^*$and x, position tracking error e_x and control input current i_q^*. (a) Existing NFTSMC: (M1). (b) TDE-based MFSMC: (M2). (c) DGTDE- MFSMC: (M3).

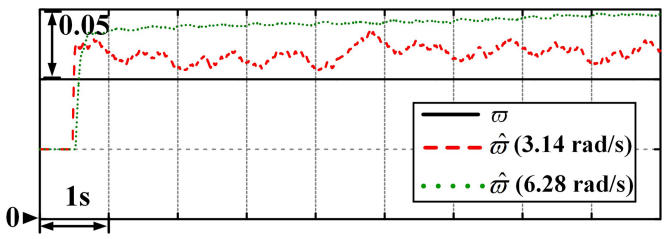

Fig. 11. Gains of TDE-based MFSMC and DGTDE-based MFSMC under parameter mismatch.

constant, the estimation performance of TDE cannot be adaptively adjusted to the optimal level based on changes in uncertainty. Thus, although TDE-based MFSMC has significantly improved steady-state tracking performance compared to NFTSMC, there is still room for further improvement.

In contrast, the TEB of DGTDE-based MFSMC is further reduced to 0.427 and 0.471 mm, as shown Figs. 6(c) and 7(c). Compared with NFTSMC and TDE-based MFSMC, these values decrease by 71.72%, 82.75% and 27.87%, 25.71%, respectively. Evidently, DGTDE-based MFSMC achieves the best steady-state tracking performance. This is due to the fact that the proposed DGTDE can adjust the gain $\hat{\varpi}$ online according to the sliding mode variable, as shown in Fig. 8. The dynamic gain $\hat{\varpi}$ at 6.28 rad/s is relatively larger than that at 3.14 rad/s. This is why the control output current in Fig. 6(c) contains more noise than Fig. 7(c). To further demonstrate the superiority of the proposed method, we have added quantitative analysis based on the minimum standard deviation (MSD) and mean (MEA) of tracking error. The analysis data are summarized in Tables III and IV. It is not difficult to see that the proposed DFTDE-based MFSMC method performs best in all three indicators.

TABLE III
QUANTITATIVE ANALYSIS RESULTS OF FIG. 6

Methods	TED (m)	MEA (m)	MSD (m)
M1	1.51e-3	1.01e-4	3.35e-4
M2	5.92e-4	2.44e-6	1.11e-4
M3	4.27e-4	1.71e-7	8.75e-5

TABLE IV
QUANTITATIVE ANALYSIS RESULTS OF FIG. 7

Methods	TED (m)	MEA (m)	MSD (m)
M1	2.73e-3	1.78e-4	4.90e-4
M2	6.34e-4	1.29e-5	1.21e-4
M3	4.71e-4	4.10e-6	1.08e-4

TABLE V
QUANTITATIVE ANALYSIS RESULTS OF FIG. 9

Methods	TED (m)	MEA (m)	MSD (m)
M1	5.66e-3	5.72e-4	1.31e-3
M2	6.74e-4	8.08e-6	1.16e-4
M3	4.45e-4	1.74e-6	8.24e-5

TABLE VI
QUANTITATIVE ANALYSIS RESULTS OF FIG. 10

Methods	TED (m)	MEA (m)	MSD (m)
M1	2.94e-3	1.40e-4	4.46e-4
M2	7.28e-4	1.84e-5	1.44e-4
M3	5.14e-4	7.61e-6	1.02e-4

C. Robustness Performance Verification

In practical applications, the parameters of PMLSM will inevitably change due to payload variations, mechanical wear and magnetic saturation. Figs. 9, 10, and 11 show the experimental results of three methods in the case of parameter mismatch ($\Delta M = M$, $\Delta K_f = 0.2K_f$, $\Delta G_c = G_c$, and $\Delta G_b = G_b$). From Figs. 9(a) and 10(a), the TEB of NFTSMC has increased to 5.66 and 2.94 mm at 6.28 and 3.14 rad/s, respectively. Obviously, the additional uncertainty caused by parameter mismatch seriously reduces the tracking performance of NFTSMC. This is also the limitation of NFTSMC based on model design, which has been analyzed in detail in Section III-A. By contrast, the TEB of TDE-based MFSMC and DGTDE-based MFSMC are 0.674 mm, 0.728 mm and 0.445 mm, 0.514 mm, as shown in Figs. 9(b), 10(b), 9(c) and 10(c), which decreased by 88.09%,75.24% and 92.13%,82.52% compared to NFTSMC. It implies that the model-free control efforts provided by TDE-based MFSMC and DGTDE-based MFSMC effectively enhance the robustness of the system to parameter changes. In addition, DGTDE-based MFSMC can also respond to changes in lumped uncertainty by adjusting its gain $\hat{\varpi}$ online, as shown in Fig. 11. This feature further overcomes the disadvantage of constant gain ϖ in TDE-based MFSMC. The quantitative analysis of tracking errors is summarized in Tables V and VI.

D. Strong Nonlinear Applicability Verification

To make the nonlinear effect of friction more pronounced, we employed a triangular command signal with an amplitude of 0.1m and a period of 2 s. The corresponding experimental results are shown in Fig. 12. In Fig. 12(a), it can be observed that the existing NFTSMC generates a maximum instantaneous tracking error of 4.84 mm due to the sudden change in velocity direction. Conversely, in Fig. 12(b), the TDE-based MFSMC exhibits a maximum instantaneous error of 3.57 mm, representing a reduction of 26.23%. Remarkably, the DGTDE-based MFSMC demonstrates its adaptability to nonlinear friction during sudden speed reversals, as shown in Fig. 12(c). It achieves this by promptly adjusting the gain $\hat{\varpi}$ in response to error variations. As a result of this adaptive mechanism, the DGTDE-based MFSMC achieves further improvements, resulting in a maximum instantaneous error of 2.62 mm. These results unequivocally establish the effectiveness of the proposed method in adapting to diverse types of position reference signals, thereby rendering it suitable for a wider range of applications in PMLSM servo control.

E. Antiexternal Disturbance Performance Verification

To further verify the ability of this method to suppress external interference, a 30N external impact force was applied in the opposite direction of the motor rotor motion through a cylinder. The corresponding experimental results are shown in Fig. 13. From Fig. 13(a) and (b), the maximum position errors of NFTSMC and TDE-based MFSMC caused by shock disturbance are 2.51 and 1.22 mm, respectively. Therefore, although the position fluctuation of TDE-based MFSMC is better than that of NFSMC, there is still a significant position error. By contrast, DGTDE-based MFSMC can operate stably, as shown in Fig. 13(c). The maximum error under shock disturbance is reduced to 0.69 mm. Moreover, when the sliding mode variable changes due to the shock disturbance, the adaptive gain $\hat{\varpi}$ increases accordingly and decreases gradually when the disturbance disappears. Therefore, DGTDE-based MFSMC can effectively improve the position tracking accuracy of PMLSM in the transient process.

F. Computing Effort Assessment

Fig. 14 shows the execution time during the digital implementation of three control methods. The control period of position loop in this article is 300 μs. It can be seen that the execution time of the existing NFTSMC method is 32.5 μs, significantly higher than the 14.8 μs of TDE-based MFSMC and the 20.3 μs of DGTDE-based MFSMC. This discrepancy can be primarily attributed to the elimination of online parameter identification processes in the MFSMC approach. These findings indicate that the model-free structure of the proposed method incurs a lower computational burden, making it a more favorable option for engineering applications. The execution time of DGTDE-based MFSMC is slightly higher than that of TDE-based MFSMC due to the additional dynamic gain calculation in (28). Despite the increased computational cost of DGTDE-MFSMC, it offers superior position tracking performance, which remains acceptable within precision PMLSM servo applications.

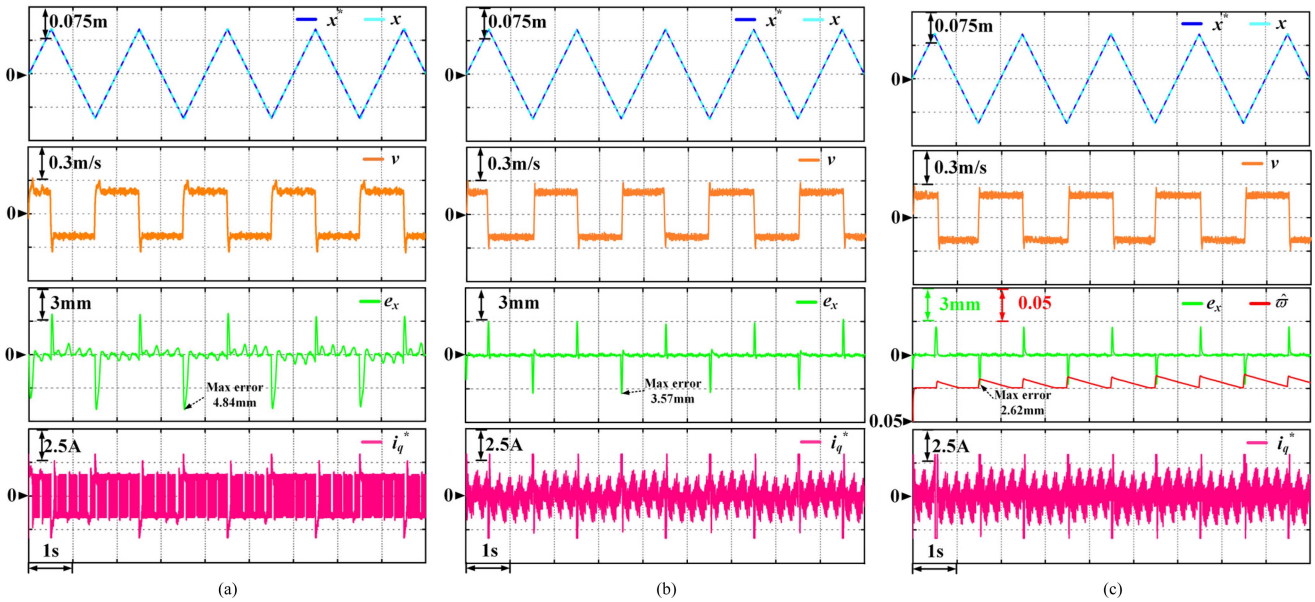

Fig. 12. Experimental results of three methods under triangular trajectories. From top to bottom: position trajectory $x^*$and x, sliding mode variable s_x and control input current i_q^*. (a) Existing NFTSMC: (M1). (b) TDE-based MFSMC: (M2). (c) DGTDE- MFSMC: (M3).

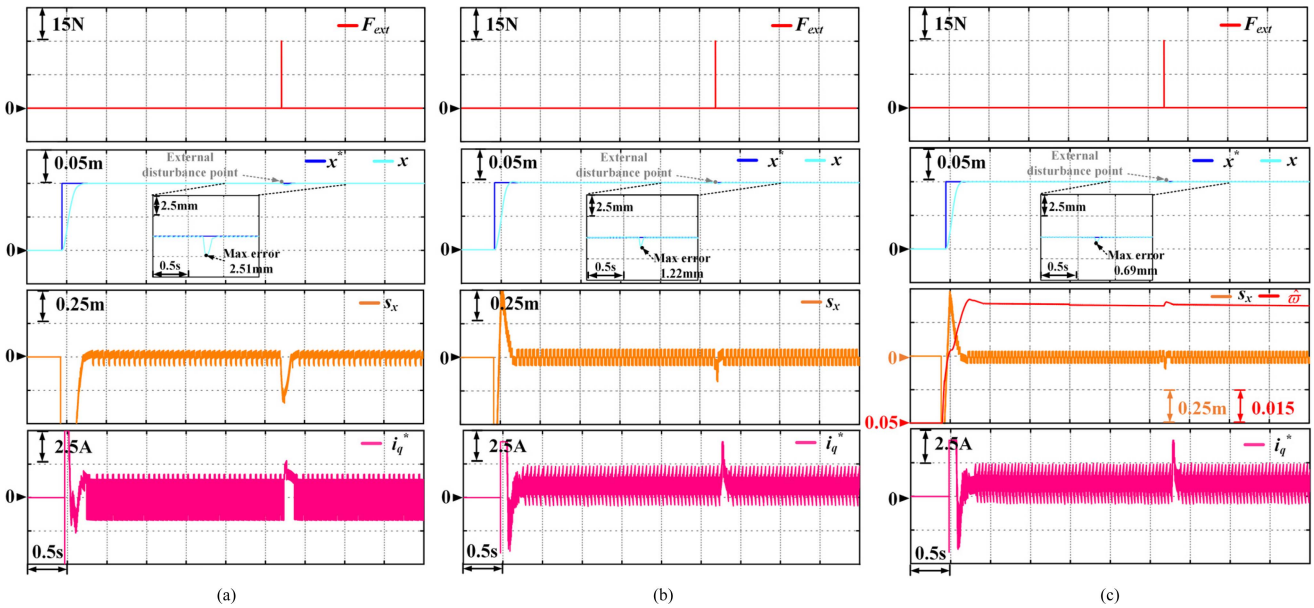

Fig. 13. Experimental results of three methods under external disturbance. From top to bottom: position trajectory $x^*$and x, sliding mode variable s_x and control input current i_q^*. (a) Existing NFTSMC: (M1). (b) TDE-based MFSMC: (M2). (c) DGTDE- MFSMC: (M3).

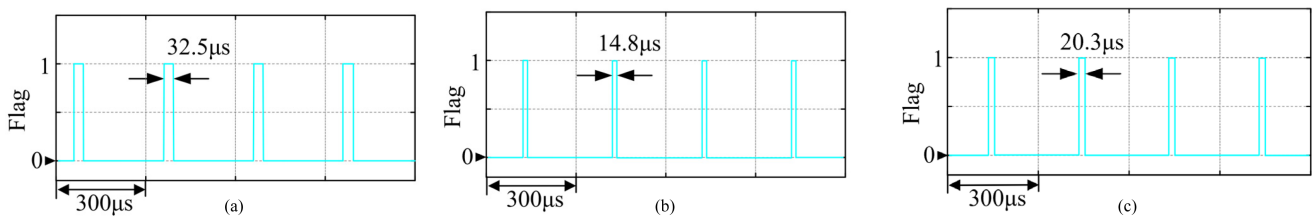

Fig. 14. Execution time of the three methods. (a) Existing NFTSMC: (M1). (b) TDE-based MFSMC: (M2). (c) DGTDE- MFSMC: (M3).

VI. Conclusion

This article proposes a DGTDE-based MFSMC for PMLSM position loop. The established abstract order model eliminates the motor parameters and nonlinear terms in conventional PMLSM dynamic models, providing a foundation for MFSMC design. Moreover, the proposed DGTDE can adjust the control gain online to achieve better tracking performance than TDE with constant gain. On the one hand, to achieve higher tracking accuracy, the dynamic gain increases when moving away from the sliding mode manifold. On the other hand, to avoid the poor transient response caused by too large gain and to reduce the influence of noise, the dynamic gain is reduced near the sliding mode manifold. The designed dynamic gain responds immediately to tracking errors through a symbolic function. The comparative experimental results also show that the proposed method is superior to the existing NFTSMC and original TDE-based MFSMC in tracking accuracy, parameter robustness and antiexternal disturbance.

The DGTDE-based MFSMC proposed in this article can adjust the control gain online based on the system tracking error. However, the adaptive gain change rate is relatively low when the sliding mode variable is reduced, and it cannot respond quickly when the load is removed. Therefore, future work will focus on designing a dynamic gain adjustment scheme with a faster adaptive rate.

Appendix A

Recalling (14) and (22), the TDE error can be rewritten as

$$\varepsilon = \varpi\ddot{x} + u \tag{45}$$

where $u = \varpi(-\ddot{x}^* + \alpha\dot{e}_x + \beta\lambda|(e_x)|^{\lambda-1}\dot{e}_x + k'_1 s_x + k'_2 \text{sign}(s_x))$.

By substituting (45) into (5), the dynamic model of PMLSM servo system with respect to ε can be obtained as follows

$$M\varepsilon = Mu + \varpi K_f i_q^* + \rho \tag{46}$$

where $\rho = -\hat{\varpi}(G_b v + G_c \text{sign}(v) + d)$.

Then, by substituting (29) into (46), the dynamic model in (49) can be rewritten as

$$M\varepsilon = (M - \varpi K_f)\, u + \varpi K_f i^*_{q(t-T_s)} - \varpi^2 K_f \ddot{x}\,(t - T_s) + \rho. \tag{47}$$

Further substitute $\ddot{x}(t - T_s)$ and $i^*_{q(t-T_s)}$ from (46) and (47) to get

$$M\varepsilon = (M - \varpi K_f)\, u + (M - \varpi K_f)\left(\varepsilon_{(t-T_s)} - u_{(t-T_s)}\right) + \rho - \rho_{(t-T_s)}. \tag{48}$$

To facilitate the analysis, TDE errors can be reorganized as follows:

$$\varepsilon = (1 - K_f\varpi/M)\,\varepsilon_{(t-T_s)} + (1 - K_f\varpi/M)\,\Delta u + \Delta\rho \tag{49}$$

where $\Delta u = u - u_{(t-T_s)}$, $\Delta\rho = \rho - \rho_{(t-T_s)}$.

Correspondingly, the discretized form of (49) is expressed as follows:

$$\varepsilon(k) = (1 - K_f\varpi/M)\,\varepsilon(k-1) + (1 - K_f\varpi/M)\,\Delta u(k) + \Delta\rho(k) \tag{50}$$

where k represents the kth sampling period.

Obviously, the conditions for the asymptotic convergence of the first-order discrete difference equation in (50) are

$$|1 - K_f\varpi/M| < 1. \tag{51}$$

Then the TDE error is bounded by $|\varepsilon| \le \Lambda$, where Λ is a positive constant. So far, the boundedness of TDE error has been proved.

Appendix B

Proof of Lemma 1: Assuming $|s_x| > \sigma$, the dynamic gain $\hat{\varpi}$ will continues to increase and drive e_x to gradually decrease. When e_x is small enough, s_x satisfies $|s_x| < \sigma$ at t_1. In this case, sign($|s_x|$-σ) $= -1$, $\hat{\varpi}$ begins to decrease continuously. This dynamic will cause e_x and s_x to begin to increase again. Then, the change in $\hat{\varpi}$ will repeat the previous pattern of change. Thus, there is an upper bound on the dynamic gain $\hat{\varpi}$ when $t > 0$. That is, there always exits a positive number $\bar{\varpi} > \hat{\varpi}$.

This completes the proof. ■

Appendix C

Consider the first-order nonlinear differential inequality given by

$$\dot{V}(x) + \eta V^{\gamma}(x) \le 0 \tag{52}$$

where $V(x)$ represents a positive Lyapunov function with respect to the state $x \in R$, $\eta > 0$, $0 < \gamma < 1$. It can be deduced that for any given initial condition $V(x(0)) = V(0)$, the function $V(x)$ converges to the origin in the finite time given by

$$t \le \frac{V^{1-\gamma}(0)}{\eta(1-\gamma)} \tag{53}$$

The derivation is referred to [36], [37] and references therein.

References

[1] M. A. M. Cheema, J. E. Fletcher, D. Xiao, and M. F. Rahman, "A linear quadratic regulator-based optimal direct thrust force control of linear permanent-magnet synchronous motor," *IEEE Trans. Ind. Electron.*, vol. 63, no. 5, pp. 2722–2733, May 2016.

[2] G. Lv, T. Zhou, and D. Zeng, "Design of ladder-slit secondaries and performance improvement of linear induction motors for urban rail transit," *IEEE Trans. Ind. Electron.*, vol. 65, no. 02, pp. 1187–1195, Feb. 2018.

[3] R. Yang, L. Li, M. Wang, and C. Zhang, "Force ripple compensation and robust predictive current control of PMLSM using augmented generalized proportional–integral observer," *IEEE J. Emerg. Sel. Topics Power Electron.*, vol. 9, no. 1, pp. 302–315, Feb. 2021.

[4] D. Xu, B. Ding, B. Jiang, W. Yang, and P. Shi, "Nonsingular fast terminal sliding mode control for permanent magnet linear synchronous motor via high-order super-twisting observer," *IEEE/ASME Trans. Mechatron.*, vol. 27, no. 3, pp. 1651–1659, Jun. 2022.

[5] S. Thomsen, N. Hoffmann, and F. W. Fuchs, "PI control, PI-based state space control, and model-based predictive control for drive systems with elastically coupled loads—A comparative study," *IEEE Trans. Ind. Electron.*, vol. 58, no. 8, pp. 3647–3657, Aug. 2011.

[6] F. Song, Y. Liu, J.-X. Xu, X. Yang, P. He, and Z. Yang, "Iterative learning identification and compensation of space-periodic disturbance in PMLSM systems with time delay," *IEEE Trans. Ind. Electron.*, vol. 65, no. 9, pp. 7579–7589, Sep. 2018.

[7] S.-D. Huang, G.-Z. Cao, J. Xu, Y. Cui, C. Wu, and J. He, "Predictive position control of long-stroke planar motors for high-precision positioning applications," *IEEE Trans. Ind. Electron.*, vol. 68, no. 1, pp. 796–811, Jan. 2021.

[8] S.-Y. Chen, H.-H. Chiang, T.-S. Liu, and C.-H. Chang, "Precision motion control of permanent magnet linear synchronous motors using adaptive fuzzy fractional-order sliding-mode control," *IEEE/ASME Trans. Mechatron.*, vol. 24, no. 2, pp. 741–752, Apr. 2019.
[9] W. Xu, S. Qu, and C. Zhang, "Fast terminal sliding mode current control with adaptive extended state disturbance observer for PMSM system," *IEEE J. Emerg. Sel. Topics Power Electron.*, vol. 11, no. 1, pp. 418–431, Feb. 2023.
[10] Z. Man and X. Yu, "Terminal sliding mode control of MIMO linear systems," *IEEE Trans. Circuits Syst. I, Reg. Papers.*, vol. 44, no. 11, pp. 1065–1070, Nov. 1997.
[11] Y. Feng, X. Yu, and Z. Man, "Non-singular terminal sliding mode control of rigid manipulators," *Automatica*, vol. 38, no. 12, pp. 2159–2167, Dec. 2002.
[12] H. Du, X. Chen, G. Wen, X. Yu, and J. Lü, "Discrete-time fast terminal sliding mode control for permanent magnet linear motor," *IEEE Trans. Ind. Electron.*, vol. 65, no. 12, pp. 9916–9927, Dec. 2018.
[13] B. Xu, L. Zhang, and W. Ji, "Improved non-singular fast terminal sliding mode control with disturbance observer for PMSM drives," *IEEE Trans. Trans. Electrific.*, vol. 7, no. 4, pp. 2753–2762, Dec. 2021.
[14] D. Fu and X. Zhao, "A novel robust adaptive nonsingular fast integral terminal sliding mode controller for permanent magnet linear synchronous motors," *IEEE J. Emerg. Sel. Topics Power Electron*, vol. 11, no. 2, pp. 1672–1683, Apr. 2023.
[15] Y. Feng, F. Han, and X. Yu, "Chattering free full-order sliding-mode control," *Automatica*, vol. 50, no. 4, pp. 1310–1314, Apr. 2014.
[16] K. Shao, J. Zheng, H. Wang, X. Wang, R. Lu, and Z. Man, "Tracking control of a linear motor positioner based on barrier function adaptive sliding mode," *IEEE Trans. Ind. Inform.*, vol. 17, no. 11, pp. 7479–7488, Nov. 2021.
[17] S. Di Gennaro, J. Rivera Domínguez, and M. A. Meza, "Sensorless high order sliding mode control of induction motors with core loss," *IEEE Trans. Ind. Electron.*, vol. 61, no. 6, pp. 2678–2689, Jun. 2014.
[18] W. Xu, A. K. Junejo, Y. Liu, M. G. Hussien, and J. Zhu, "An efficient antidisturbance sliding-mode speed control method for PMSM drive systems," *IEEE Trans. Power Electron.*, vol. 36, no. 6, pp. 6879–6891, Jun. 2021.
[19] D. Fu, X. Zhao, and J. Zhu, "A novel robust super-twisting nonsingular terminal sliding mode controller for permanent magnet linear synchronous motors," *IEEE Trans. Power Electron.*, vol. 37, no. 3, pp. 2936–2945, Mar. 2022.
[20] K. Youcef-Toumi and O. Ito, "A time delay controller design for systems with unknown dynamics," *Trans. ASME J. Dyn. Syst. Meas. Control*, vol. 112, no. 1, pp. 133–142, Mar. 1990.
[21] Y. Kali et al., "Time delay estimation based discrete-time super-twisting current control for a six-phase induction motor," *IEEE Trans. Power Electron.*, vol. 35, no. 11, pp. 12570–12580, Nov. 2020.
[22] L. Wang, J. Zhao, Z. Yu, Z. Pan, and Z. Zheng, "Robust and high-precision position control of PMLSM-driven feed servo system based on adaptive fast nonsingular terminal sliding mode," *IEEE Trans. Trans. Electrific.*, vol. 11, no. 1, pp. 4882–4894, Feb. 2025.
[23] S. Li, M. Zhou, and X. Yu, "Design and implementation of terminal sliding mode control method for PMSM speed regulation system," *IEEE Trans. Ind. Inform.*, vol. 9, no. 4, pp. 1879–1891, Nov. 2013.
[24] L. Yang and J. Yang, "Nonsingular fast terminal sliding-mode control for nonlinear dynamical systems," *Int. J. Robust Nonlinear Control*, vol. 21, no. 16, pp. 1865–1879, 2011.
[25] W. Gao and J. C. Hung, "Variable structure control of nonlinear systems: A new reach," *IEEE Trans. Ind. Electron.*, vol. 40, no. 1, pp. 45–55, Feb. 1993.
[26] G. F. Franklin, J. Powell, and M. Workman, *Digital Control of Dynamic Systems*. Reading, MA, USA: Addison-Wesley, 1998.
[27] M. Jin, S. H. Kang, and P. H. Chang, "Robust compliant motion control of robot with nonlinear friction using time-delay estimation," *IEEE Trans. Ind. Electron.*, vol. 55, no. 1, pp. 258–269, Jan. 2008.
[28] T. C. Hsia and L. S. Gao, "Robot manipulator control using decentralized linear time-invariant time-delayed joint controllers," in *Proc. IEEE Int. Conf. Robot. Autom.*, 1990, pp. 2070–2075.
[29] L. Wang, J. Zhao, Z. Yu, Z. Pan, and Z. Zheng, "High-precision position control of PMLSM using fast recursive terminal sliding mode with disturbance rejection ability," *IEEE Trans. Ind. Inform.*, vol. 20, no. 2, pp. 2577–2588, Feb. 2024.
[30] K. Shao, J. Zheng, K. Huang, H. Wang, Z. Man, and M. Fu, "Finite-time control of a linear motor positioner using adaptive recursive terminal sliding mode," *IEEE Trans. Ind. Electron.*, vol. 67, no. 8, pp. 6659–6668, Aug. 2020.
[31] H. Dong, X. Yang, and M. V. Basin, "Practical tracking of permanent magnet linear motor via logarithmic sliding mode control," *IEEE/ASME Trans. Mechatron.*, vol. 27, no. 5, pp. 4112–4121, Oct. 2022.
[32] K. Zhang, L. Wang, and X. Fang, "High-order fast nonsingular terminal sliding mode control of permanent magnet linear motor based on double disturbance observer," *IEEE Trans. Ind. Appl.*, vol. 58, no. 3, pp. 3696–3705, May/Jun. 2022.
[33] L. Wang, J. Zhao, and Z. Zheng, "Robust speed tracking control of permanent magnet synchronous linear motor based on a discrete-time sliding mode load thrust observer," *IEEE Trans. Ind. Appl.*, vol. 58, no. 4, pp. 4758–4767, Jul./Aug. 2022.
[34] J. Lin, W. Jiang, L. Zhou, J. Sun, and X. Song, "Improved model-free sliding mode control of linear motor based on time-varying gain model-assisted linear extended state observer," *IEEE Access*, vol. 12, pp. 20726–20733, 2024.
[35] J. Zheng, H. Wang, Z. Man, J. Jin, and M. Fu, "Robust motion control of a linear motor positioner using fast nonsingular terminal sliding mode," *IEEE/ASME Trans. Mechatron.*, vol. 20, no. 4, pp. 1743–1752, Aug. 2015.
[36] E. Moulay and W. Perruquetti, "Finite time stability and stabilization of a class of continuous systems," *J. Math. Anal. Appl.*, vol. 323, no. 2, pp. 1430–1443, Nov. 2006.
[37] F. Plestan, Y. Shtessel, V. Bregeault, and A. Poznyak, "New methodologies for adaptive sliding mode control," *Int. J. Control*, vol. 83, no. 9, pp. 1907–1919, Sep. 2010.

Lijun Wang was born in Chuzhou, China. He received the B.S. degree in electrical engineering and automation and the M.S. degree in detection technology and automatic equipment from Anhui University, Hefei, China, in 2016 and 2019, respectively, and the Ph.D. degree in electrical engineering from Hefei University of Technology, Hefei, China, in 2024.

Since July, 2024, he has been a Lecturer with the School of Internet, Anhui University, Hefei, China. His current research focuses on linear motor control and multimotor collaborative control.

Jiwen Zhao (Senior Member, IEEE) was born in Dangshan, China. He received the Ph.D. degree in precision machinery and instruments from the University of Science and Technology of China, Hefei, China, in 2005.

Since 2019, he has been working with the School of Electrical and Automation Engineering, Hefei University of Technology, Hefei, China. He is currently a Professor with the School of Electrical and Automation Engineering, Hefei University of Technology, Hefei, China. His research interests include linear motor optimization design, linear motor control and photoelectric detection technology.

Juncai Song (Member, IEEE) was born in Huainan, China. He received the Ph.D. degree in electronic information from Anhui University, Hefei, China, in 2020.

Since 2024, he has been an Associate Professor with the School of Internet, Anhui University, Hefei, China. His current research interests include electric motor fault diagnosis, design optimization in linear motors and power quality disturbance identification.

Zixiang Yu (Member, IEEE) was born in Liaoning, China, in 1993. He received the B.E.E. degree in electrical engineering, from Dalian Maritime University, Dalian, China, in 2015, and the M.S. and Ph.D. degrees in electrical engineering, from Huazhong University of Science &Technology, Wuhan, China, in 2018 and 2021, respectively.

Since July, 2021, he has been an Associate Professor in electrical engineering, with the School of Electrical Engineering and Automation, Hefei University of Technology, Hefei, China. His current research focuses on control strategy of PM machines, reluctance machines, and multiphase machines.

Zhenbao Pan (Member, IEEE) was born in Guilin, China. He received the B.S. degree in electrical engineering and automation and the M.S. degree in detection technology and automatic equipment from Anhui University, Hefei, China, in 2014 and 2017, respectively, and the Ph.D. degree in electrical engineering from Southeast University, Nanjing, China, in 2022.

Since 2022, he has been with Hefei University of Technology, where he is currently a Lecturer with the School of Electrical Engineering and Automation. His main research interests include design, analysis, optimization and control of permanent-magnet motors with particular reference to permanent-magnet linear motors and permanent-magnet arc motors.